ELectronics EXpress

LETTER

IEICE Electronics Express, Vol.14, No.11, 1–11

Adjustable SQUID-resonator direct coupling in microwave SQUID multiplexer for TES microcalorimeter array

Yuki Nakashima[1,2a)], **Fuminori Hirayama**[2], **Satoshi Kohjiro**[2], **Hirotake Yamamori**[2], **Shuichi Nagasawa**[2], **Noriko Y. Yamasaki**[1], **and Kazuhisa Mitsuda**[1]

[1] *Institute of Space and Astronautical Science (ISAS), Japan Aerospace Exploration Agency (JAXA), 3–1–1 Yoshinodai, Sagamihara, Kanagawa 229–8510, Japan*

[2] *National Institute of Advanced Industrial Science and Technology (AIST), 1–1–1 Umezono, Tsukuba, Ibaraki 305–8568, Japan*

a) *nakasima@astro.isas.jaxa.jp*

Abstract: We have succeeded in the first demonstration of a simple and accurate resonator-superconducting quantum interference device (SQUID) coupling for microwave SQUID multiplexers. A simple theory shows our direct coupling with adjustable fractional inductance in the SQUID loop can decrease the deviation of resonance frequencies from designed values in contrast to a conventional inductive coupling. Our direct coupling provides the individual coupling that can be optimized with keeping identical structure, shape, and dimension of the SQUID among all pixels on the same chip. It covers experimentally three or potentially more factors of a frequency band that is larger than that of cryogenic high electron mobility transistor amplifiers. The deviation of experimental fractional inductance from the designed one is less than −3/+10%.

Keywords: microwave SQUID multiplexer, SQUID readout, microwave resonators, superconducting transition edge sensors (TES), microcalorimeters

Classification: Superconducting electronics

References

[1] S. J. Smith, *et al.*: "Small pitch transition-edge sensors with broadband high spectral resolution for solar physics," J. Low Temp. Phys. **167** (2012) 168 (DOI: 10.1007/s10909-012-0574-y).

[2] D. Schwan, *et al.*: "APEX-SZ a Sunyaev-Zel'dovich galaxy cluster survey," New Astron. Rev. **47** (2003) 933 (DOI: 10.1016/j.newar.2003.09.008).

[3] K. Mitsuda: "TES X-ray microcalorimeters for X-ray astronomy and material analysis," Physica C **530** (2016) 93 (DOI: 10.1016/j.physc.2016.03.018).

[4] R. D. Horansky, *et al.*: "Superconducting calorimetric alpha particle sensors for nuclear nonproliferation applications," Appl. Phys. Lett. **93** (2008) 123504 (DOI: 10.1063/1.2978204).

DOI: 10.1587/elex.14.20170271
Received March 21, 2017
Accepted May 2, 2017
Publicized May 22, 2017
Copyedited June 10, 2017

[5] J. N. Ullom and D. A. Bennett: "Review of superconducting transition-edge sensors for x-ray and gamma-ray spectroscopy," Supercond. Sci. Technol. **28** (2015) 084003 (DOI: 10.1088/0953-2048/28/8/084003).
[6] J. A. B. Mates, *et al.*: "Demonstration of a multiplexer of dissipationless superconducting quantum interference devices," Appl. Phys. Lett. **92** (2008) 023514 (DOI: 10.1063/1.2803852).
[7] O. Noroozian, *et al.*: "High-resolution gamma-ray spectroscopy with a microwave-multiplexed transition-edge sensor array," Appl. Phys. Lett. **103** (2013) 202602 (DOI: 10.1063/1.4829156).
[8] A. Giachero, *et al.*: "Development of microwave-multiplexed superconductive detectors for the HOLMES experiment," J. Phys. Conf. Ser. **718** (2016) 062020 (DOI: 10.1088/1742-6596/718/6/062020).
[9] P. K. Day, *et al.*: "A broadband superconducting detector suitable for use in large arrays," Nature **425** (2003) 817 (DOI: 10.1038/nature02037).
[10] F. Hirayama, *et al.*: "Microwave SQUID multiplexer for TES readout," IEEE Trans. Appl. Supercond. **23** (2013) 2500405 (DOI: 10.1109/TASC.2012.2237474).
[11] J. A. B. Mates: "The microwave SQUID multiplexer," Ph.D thesis, the University of Colorado (2011).
[12] S. Kempf, *et al.*: "Demonstration of a scalable frequency-domain readout of metallic magnetic calorimeters by means of a SQUID multiplexers," AIP Adv. **7** (2017) 015007 (DOI: 10.1063/1.4973872).
[13] B. L. Zink, *et al.*: "Array-compatible transition-edge sensor microcalorimeter γ-ray detector with 42 eV energy resolution at 103 keV," Appl. Phys. Lett. **89** (2006) 124101 (DOI: 10.1063/1.2352712).
[14] A. Giachero, *et al.*: "Development of multiplexed rf-SQUID based micro-calorimeter detectors for the HOLMS experiment," Applied Superconductivity Conference (2016) 1EOr2C-06.
[15] K. D. Irwin, *et al.*: "Thermal-response time of superconducting transition-edge microcalorimeters," J. Appl. Phys. **83** (1998) 3978 (DOI: 10.1063/1.367153).
[16] LOW NOISE FACTORY: http://www.lownoisefactory.com.
[17] W. H. Chang: "The inductance of a superconducting strip transmission line," J. Appl. Phys. **50** (1979) 8129 (DOI: 10.1063/1.325953).
[18] C. Kittel: *Introduction to Solid State Physics* (Wiley, Hoboken, 2004) 8th ed. 275.

1 Introduction

Superconducting transition-edge sensors (TES) are the most sensitive calorimeters or bolometers. For example, state-of-the-art TES X-ray detectors achieve an energy resolution of 1.58 eV FWHM at 5.9 keV [1]. Since TES are thermal detectors, they are in principle very broadband. Thus, TES are used in various applications, over a span of more than ten orders of magnitude in wavelength and energy, including astronomy for cosmic microwave back-ground (CMB) [2], X-ray spectroscopy in material analysis [3] and nuclear and particle physics [4]. Superconducting quantum interference devices (SQUID) are suitable readout elements for TES because of their low impedances and current resolutions. For a single TES or TES array with small numbers of pixels, signal wires for output of individual SQUID corresponding to each TES pixel can be connected in parallel between the cryogenic stage and room-temperature electronics. This approach could not be scaled up to large-format

DOI: 10.1587/elex.14.20170271
Received March 21, 2017
Accepted May 2, 2017
Publicized May 22, 2017
Copyedited June 10, 2017

arrays to image and/or increase collection efficiency and count rate, since this increases the prohibitive heat flow from room-temperature to the cryogenic stage through signal and/or bias wires 8 per pixel. Thus, SQUID multiplexing techniques are potentially needed for the readout of large-format TES arrays.

For more than a decade, time-division multiplexing (TDM), code-division multiplexing (CDM), and frequency-division multiplexing (FDM) with several-MHz bandwidth [5], which allow tens of pixels to be read out in each output line, have been developed. However, there is a need for a multiplexing technique capable of reading out thousands of detectors in a single output channel. Microwave SQUID multiplexers (MW-Mux) [6, 7, 8] are attractive for such use because of their much larger bandwidth than those of three conventional methods, potentially several GHz.

MW-Mux consists of a number of high quality-factor (Q) microwave resonators, each employing a unique resonance frequency, terminated by rf-SQUID. Each SQUID acts as a flux-variable inductor responding to the magnetic flux threading the SQUID loop in a flux-quantum Φ_0 ($= 2.07 \times 10^{-15}$ Wb) cycle. Thus, a TES signal is read out by monitoring the shift of the resonance frequency depending on the magnetic flux activated by change of current though TES at energy irradiation. For multiplexing, those elements are capacitively coupled to a feedline. As with the readout system of microwave kinetic inductance detectors [9], each signal can be simultaneously obtained by injecting multiple microwave tones into the feedline and monitoring the complex value of transmitted signals.

Though MW-Mux is expected as a readout circuit of the next-generation large-format TES arrays, this broadband multiplex can be achieved only by optimizing the SQUID-resonator coupling strength to the same level at difference resonance frequencies for all channels. We have investigated MW-Mux with microstrip-type SQUID [10] which can be designed much more simply and accurately than planar SQUID used in general [11]. Also, we have proposed direct SQUID-resonator coupling with adjustable parameter in contrast to conventional inductive coupling (see Fig. 1). This has, however, never been demonstrated before. In this paper, we report the first demonstration that the SQUID-resonator coupling strength can be optimized simply and accurately by varying only the position of ground via on the microstrip loop for all channels.

2 Theory and design

2.1 Direct SQUID-resonator coupling with adjustable fractional inductance

Fig. 1 shows equivalent circuit of the main part of MW-Mux. The output current of each TES pixel is read by a corresponding SQUID of the self inductance L_S with the mutual inductance M_{in}. The SQUID is coupled either inductively (Fig. 1(a)) or directly (Fig. 1(b)) to a quarter-wavelength resonator based on a superconducting coplanar waveguide (CPW) with the characteristic impedance $Z_0 = 50\,\Omega$. The input ports of all resonators are connected to a CPW microwave feedline through coupling capacitors C_C. The output port of the feedline is terminated by a cryogenic high-electron mobility transistor (HEMT) amplifier that is usually positioned at a

DOI: 10.1587/elex.14.20170271
Received March 21, 2017
Accepted May 2, 2017
Publicized May 22, 2017
Copyedited June 10, 2017

~4 K stage that handles much larger power consumption than a ~0.1 K stage for TES and MW-Mux chips. When the frequency of the input microwave f_{MW} is either much larger or smaller than the resonance frequency of any resonator f_r, the microwave is not disturbed by resonators and transmitted to the HEMT amplifier. In contrast, for $f_{MW} \approx f_r$, the feedline is short-circuited by series of C_C and corresponding resonator, resulting in the reflection of the microwave. This provides the same number of dips as that of TES pixels in the frequency-transmission characteristic of the MW-Mux. The frequency position of the dip f_r is modulated by the output current of the corresponding TES pixel. Thus, one can simultaneously know the signal energy arriving at all TES pixels by means of the shift of amplitude and phase of the microwave frequency comb signals from the input port of feedline.

The difference between inductive coupling (Fig. 1(a)) and direct one (Fig. 1(b)) is the inductance terminating the resonator L_L, i.e. $L_L = L_{LMC}$ and $L_L = L_{LDI}$, respectively. For the inductive coupling,

$$L_{LMC} = L_{MW} - \frac{\eta_{MC}{}^2 L_S{}^2}{L_S + L_J} \tag{1}$$

where L_{MW} is the self inductance of coil for SQUID-resonator coupling, $\eta_{MC} \equiv M/L_S$ the degree of inductive coupling between SQUID and resonator, M the mutual inductance that manages its coupling, and $L_J = L_{J0}\sec(2\pi\Phi/\Phi_0)$ is the Josephson inductance originated from the behavior of the Josephson junction as a function of the magnetic flux threading the SQUID loop Φ. Here, let I_C be the critical current of the junction, then L_{J0} can be written in the form $L_{J0} = \Phi_0/(2\pi I_C)$. For the direct coupling,

$$L_{LDI} = \eta_{DI} L_S - \frac{\eta_{DI}{}^2 L_S{}^2}{L_S + L_J} \tag{2}$$

where $\eta_{DI} \equiv (1 - a)$ is the degree of direct coupling between SQUID and resonator, and a $(0 \le a \le 1)$ is a fractional parameter of the SQUID-loop inductance shown in Fig. 1(b). From Eq. (1) and Eq. (2) under the condition of $\eta_{MC} = \eta_{DI} \equiv \eta$, the difference of termination inductance of resonator in two regimes is given by

$$L_{LMC} - L_{LDI} = L_{MW}\left(1 - \eta\frac{L_S}{L_{MW}}\right). \tag{3}$$

Under $\eta \le 1$ and the usual condition of $L_S \ll L_{MW}$ and $L_{LMC} \approx L_{MW}$, one can get $L_{LDI} \approx L_{LMC} - L_{MW} \ll L_{LMC}$. This is valid for three examples in Mates (2011) [11] in which Tables 7.1, 7.2, and 7.3 provides $L_{MW} = 77.6$, 145 and 186 pH and $\eta L_S = M = 1.65$, 9.42 and 5.46 pH and resulting $(L_{LMC} - L_{LDI})/L_{MW} = 0.978$, 0.938 and 0.973, respectively.

The terminal inductance L_L that is not negligibly small can cause the variation of resonant frequency. According to Mates (2011) [11], the resonant frequency of MW-Mux is given by

$$f_r = \frac{f_{\frac{\lambda}{4}}}{1 + 4f_{\frac{\lambda}{4}}C_C Z_0 + 4f_{\frac{\lambda}{4}}L_L/Z_0} \tag{4}$$

where $f_{\frac{\lambda}{4}}$ is the frequency at which the resonator length is equal to the quarter wavelength. Eq. (4) means that f_r deviates from $f_{\frac{\lambda}{4}}$ due to C_C or L_L by fractions of

DOI: 10.1587/elex.14.20170271
Received March 21, 2017
Accepted May 2, 2017
Publicized May 22, 2017
Copyedited June 10, 2017

about $4f_{\frac{\lambda}{4}}C_C Z_0$ or $4f_{\frac{\lambda}{4}}L_L/Z_0$, respectively, when $4f_{\frac{\lambda}{4}}C_C Z_0 \ll 1$ and $4f_{\frac{\lambda}{4}}L_L/Z_0 \ll 1$. The variation of experimental f_r from designed f_r of superconducting CPW is originated from the variation of C_C and L_L. To decrease the variation due to L_L, it is desired to satisfy $L_L/Z_0 \ll C_C Z_0$. This becomes especially important when each pixel has unique shape, size, distance from SQUID ring, and resulting designed values of L_L. In general inductive coupling, the position of L_L is outside of coil that acts as coupling between TES and SQUID since $M_{in} \gg M$ is required. When each TES pixel has unique values of parameters different from some of other pixels, these pixels have several kinds of coil shape, size, distance from SQUID ring, and values of M_{in}. In this case, the design of L_L cannot be independent of inner coil for coupling between TES and SQUID. This can increase complexity of design and resulting variation of L_L. In fact, practical inductive coupling does not satisfy $L_L/Z_0 \ll C_C Z_0$, e.g., $4f_{\frac{\lambda}{4}}L_L/Z_0 \approx 4.8 \times 10^{-2}$ that is larger than $4f_{\frac{\lambda}{4}}C_C Z_0 \approx 1.2 \times 10^{-2}$ estimated from $f_{\frac{\lambda}{4}} \approx 6\,\mathrm{GHz}$, $C_C \approx 10\,\mathrm{fF}$, $L_L \approx 0.1\,\mathrm{nH}$ and $Z_0 \approx 50\,\Omega$ [11]. To decrease L_L so that $L_L/Z_0 \ll C_C Z_0$, the direct coupling is better than the inductive one.

For the proper operation of MW-Mux, Δf_r, the maximum shift of f_r when the input flux of the SQUID is gradually varied from $n\Phi_0$ to $(n+1)\Phi_0$, is important, where n is an integer. To optimize both the responsivity and dynamic range those are in "trade-off", Δf_r should be nearly equal to the full width at half maximum of the frequency-transmission characteristics under resonance f_r/Q_L, where Q_L is the loaded quality factor of a resonator. This means each SQUID should be designed to have unique value of Δf_r that depends on f_r of the corresponding resonator. More strictly, for the inductive coupling, the relation between Δf_r and f_r is given by [11]

$$\Delta f_r = \frac{4f_r^2}{Z_0}\frac{2\lambda}{1-\lambda^2}\frac{M^2}{L_S} \tag{5}$$

$$= \frac{4f_r^2}{Z_0}\frac{2\lambda}{1-\lambda^2}\eta_{MC}{}^2 L_S \tag{6}$$

where $\lambda = L_S/L_{J0}$ should be $\lambda < 1$ for the input-output characteristic without hysteresis, and our numerical simulation shows $\lambda \leq 0.6$ is desired from the view point of keeping the large signal-conversion efficiency of the SQUID.

Early direct coupling MW-Mux did not offer the functionality of adjusting the coupling between SQUID and resonator [6, 11]. We first added this functionality by introducing a fractional parameter a of a SQUID loop inductance as shown in Fig. 1(b) [10]. For the direct coupled MW-Mux, the relation between Δf_r and f_r is given by

$$\Delta f_r = \frac{4f_r^2}{Z_0}\frac{2\lambda}{1-\lambda^2}(1-a)^2 L_S$$

$$= \frac{4f_r^2}{Z_0}\frac{2\lambda}{1-\lambda^2}\eta_{DI}{}^2 L_S. \tag{7}$$

Eq. (7) becomes as same as Eq. (6) by replacing η_{MC} with η_{DI}. The restriction of $\eta_{DI} \leq 1$ may be a drawback of the direct coupling since both $\eta_{MC} \leq 1$ and $\eta_{MC} \geq 1$ are in principle possible. In the following, we explain this is not true for many applications.

DOI: 10.1587/elex.14.20170271
Received March 21, 2017
Accepted May 2, 2017
Publicized May 22, 2017
Copyedited June 10, 2017

To be clear required value of η ($= \eta_{MC}$ or η_{DI}) for several applications, in Fig. 2, we plot 4 curves on Δf_r-f_r plane which satisfy $\eta = 1$ in Eq. (6) and Eq. (7) under the condition of $\lambda = 0.3$ and $Z_0 = 50\,\Omega$. Each curve corresponds to $L_S = 5$, 10, 20, and 40 pH, while conventional works on MW-Mux [10, 11, 12] reported $3 < L_S \leq 60$ pH. The Δf_r-f_r region under these curves requires $\eta < 1$, while the region above does $\eta > 1$. TES spectrometers based on MW-Mux usually need the flux-ramp modulation [7] for its linear input-output characteristics and large dynamic range. In this regime, the resonator bandwidth f_r/Q_L should be much larger than the modulation frequency f_M and $f_M > 5/\tau_r$ for more than 5 sampling points setting at the rising part of pulse wave, where τ_r is the rise time of output pulse signal of a TES pixel under the incident of a photon that depends on its application. From these, $\Delta f_r \approx f_r/Q_L$ is designed to be in the range of $30/\tau_r < f_r/Q_L < 60/\tau_r$ for spectroscopy with energy resolving power $E/\Delta E$ roughly above 5×10^2. In Fig. 2, we put three dotted lines with unique values of $\Delta f_r \approx f_r/Q_L$: each is suitable for readout of either (1) γ-ray TES for nuclear safeguards [13], (2) X-ray TES for astronomy [3] or basic science [8], or (3) X-ray TES for industrial analysis [3]. Since required values of f_r/Q_L are independent of the readout frequency f_{MW}, all dotted lines are horizontal. We determine $\Delta f_r \approx 300$ kHz from $\tau_r \approx 0.1$ ms [13] for (1), $\Delta f_r \approx 3$ MHz from $\tau_r \approx 10\,\mu$s in our TES [3] and $\tau_r \approx 25\,\mu$s in neutrino-mass detectors developed in U.S.A. and Italy [14] for (2), and for (3), $\Delta f_r \approx 25$ MHz on the assumption of $\tau_r \approx 0.1\tau_f$ where $\tau_f \approx 10\,\mu$s [15] is the fall time of output pulse signal of a TES pixel. Fig. 2 indicates the MW-Mux with $\eta < 1$ covers applications (1) and (2) for $L_S \geq 5$ pH and $f_{MW} \geq 4$ GHz that contains the typical band of low-noise cryogenic HEMT amplifiers commercially available. Fig. 2 also shows the MW-Mux with $\eta < 1$ is applicable also for (3) with the combination of SQUID with $L_S \geq 40$ pH and a HEMT amplifier with typical 4–8 GHz band. Recently the operation band of commercial HEMT amplifiers has been extended to 4–16 GHz [16]. Taking into account of future MW-Mux systems based on such broadband HEMT amplifiers, the horizontal axis of Fig. 2 is defined from 4 to 16 GHz. Fig. 2 indicates the MW-Mux with $\eta < 1$ and $L_S = 5$ pH is applicable also for (3) when readout electronics with $f_{MW} \geq 10$ GHz is established. From Fig. 2, the direct coupling MW-Mux with restriction of $\eta < 1$ can cover many applications that needs TES calorimeters with the energy resolving power $E/\Delta E \geq 5 \times 10^2$.

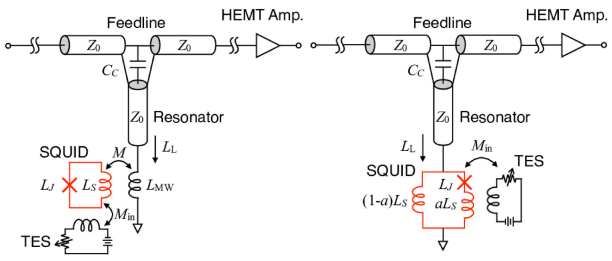

Fig. 1. Two ways of SQUID-resonator coupling. (a) Conventional inductive coupling between SQUID and resonator. (b) Advanced direct coupling we have proposed [10]. Coupling strength can be characterized by means of fractional parameter a.

DOI: 10.1587/elex.14.20170271
Received March 21, 2017
Accepted May 2, 2017
Publicized May 22, 2017
Copyedited June 10, 2017

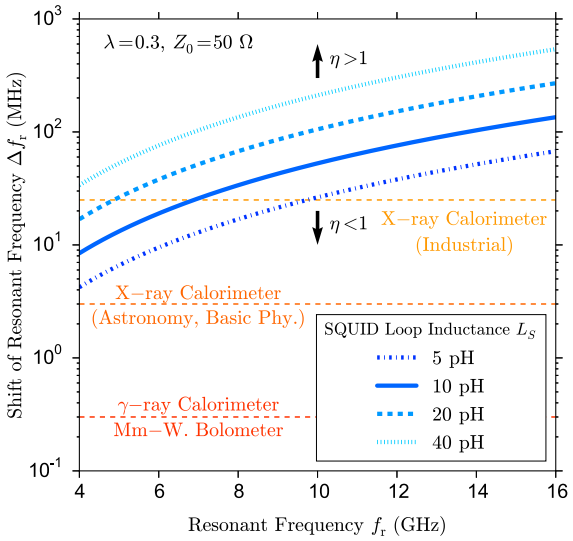

Fig. 2. Maximum shift of resonance frequency Δf_r vs. resonance frequency f_r with $\eta = 1$ and 4 values of L_S in Eqs. (6) and (7). Three horizontal dotted lines correspond to requirement that depends on application of TES (see text).

2.2 SQUID design

We designed 16-channel MW-Mux chips including test elements on which each SQUID connected to a pair of terminals to inject current on the purpose of the evaluation of aL_S, $(1-a)L_S$ and L_S [10]. The chips consists of three Nb electrode layers with SiO_2 insulation layers stacked on Si substrate, and were fabricated by Nb-based superconducting circuit technology. Critical current of the Josephson junction I_C is designed to be 10 μA, that is realized by 4 μm^2 area and 250 A/cm^2 critical current density. Each SQUID acts as a first-order parallel gradiometer which is formed by symmetric two stripline loops in parallel. Fig. 3(a) shows a photograph of one side of the two loops which consist of 20 μm wide Nb stripline on a ground plane. The loops are bended to prevent interference between adjacent channels. Each loop has two stripline coils, one is connected to the resonator via the junction and the other directly. The former and latter inductances are respectively denoted by aL_S and $(1-a)L_S$ as in Fig. 3(b).

The inductances can be varied by adjusting the length of the stripline with an inductance per unit length L_{unit} given by [17]

$$L_{unit} = \frac{\mu_0 D}{w K_f} \tag{8}$$

with

$$D \approx h + 2\lambda_L, \tag{9}$$

for our case in which the thickness of both electrodes are enough larger than λ_L. Here, μ_0, $w = 20\,\mu m$ and $K_f = 1.1$ are respectively the permeability of free space, the stripline width and the fringe coefficient. $h = 300\,nm$ and $\lambda_L = 39\,nm$ [18] are the thickness of the insulator, and the magnetic penetration depth of the electrode beneath and above the insulator, respectively. Considering the loop length l and an extra inductance L_{ext} due to L_{unit} value of the common bridge of the parallel-loop

DOI: 10.1587/elex.14.20170271
Received March 21, 2017
Accepted May 2, 2017
Publicized May 22, 2017
Copyedited June 10, 2017

gradiometer that differs from L_{unit} of the main loop, the loop inductance L_S can be written in the form

$$L_S = L_{unit} l + L_{ext}. \tag{10}$$

In our case, L_{unit} and L_{ext} are calculated as 0.011 pH/μm and 0.52 pH, respectively. To satisfy the hysteresis parameter $\lambda \approx 0.2$, we determined that the loop length is $l = 540\,\mu m$ to get the value of $L_S = 6.5$ pH. Our goal is to demonstrate that only varying the position of the ground via on the SQUID loop can optimize the fractional parameter a. For this purpose, we prepared 7 test elements which have different pairs of aL_S and $(1-a)L_S$ with common value of $l = 540\,\mu m$. Each of seven test elements has different SQUID geometry on the basis of $l_{JJ} = 161$, 210, 245, 318, 350, 459 and 466 μm, where l_{JJ} is the length from the junction to the GND defined as the red arrow running through the center of the stripline in Fig. 3(a).

To extract each pair of inductances experimentally, a pair of three terminals for current injection are connected to each SQUID of seven test elements as in Fig. 3. One is connected to the ground plane, another is connected to the point between the junction and the fractional inductance aL_S, and the other is connected to the point between the junction and the fractional inductance $(1-a)L_S$. The inductances can be extracted from periodic response of the SQUID as a function of current flowing through two of these three terminals.

In conventional inductive couplings, each pixel has unique values of M and resulting coil dimensions of L_{MW}. Especially for large-format array, this can cause the design complexity and variation from the designed L_{MW} and M. In our advanced design method, we can change fractional parameters a, keeping identical structure, shape and dimension of the SQUID for all pixels except only for varying the GND position. In our design regime, the fractional parameter a could be varied in the range from 0.04 to 0.87.

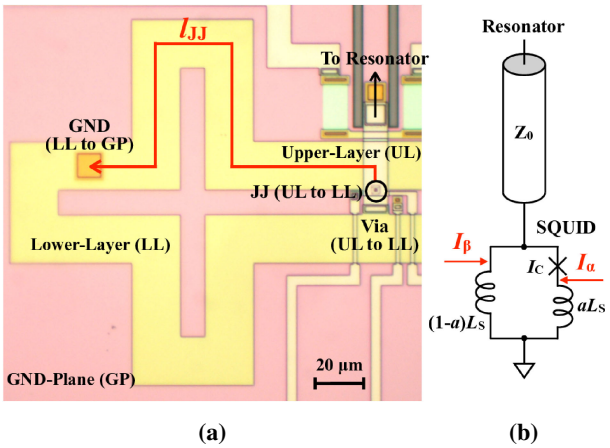

Fig. 3. (a) A photograph of SQUID fabricated for evaluation of SQUID loop and fractional inductances. The length from Josephson junction (JJ) to ground (GND) l_{JJ} is defined as the red arrow running through the center of the strip. (b) Equivalent circuit schematic of a SQUID. The two red arrows indicate current-injection points. The values of aL_S and $(1-a)L_S$ can be obtained by injecting current I_α and I_β, respectively.

DOI: 10.1587/elex.14.20170271
Received March 21, 2017
Accepted May 2, 2017
Publicized May 22, 2017
Copyedited June 10, 2017

3 Measurement and result

To validate our design in terms of a, a pair of fractional inductances aL_S and $(1-a)L_S$ was evaluated as a function of l_{JJ}. These inductances were extracted by measuring the periodic f_r-I_α and f_r-I_β relations by means of the frequency-dependent transmitted signal through the microwave feedline loaded by 7 kinds of the test-element SQUID described in section 2.2 on one of 16-channel MW-Mux chips we developed.

The chip was mounted on a sample holder that was screened with a magnetic shield and cooled in a Gifford-McMahon refrigerator down to 4 K. A microwave signal with −50 dBm from a vector network analyzer (VNA) was injected into the cryostat, damped via a 30 dB attenuator, and launched along the feedline. The transmitted signal from the chip was returned to the VNA through a cryogenic HEMT amplifier with ∼30 dB gain and ∼7 K noise temperature, and a ∼40 dB gain amplifier at room temperature. A current source at room temperature was electrically connected to the terminals on the SQUID by way of a printed circuit board attached on the sample holder. By stepwise applying a static injection current in the range from −2 to 2 mA to the terminals of each test element and acquiring transmission amplitude and phase at a fixed frequency, we obtained periodic responses of the SQUID depending on the injected current and extracted the inductances by dividing those periods by Φ_0.

Fig. 4 illustrates l_{JJ} dependence of both inductances of the fractional and total loop. Linearly with l_{JJ}, aL_S increases and $(1-a)L_S$ decreases. From the slope of aL_S-l_{JJ} and $(1-a)L_S$-l_{JJ} relations, L_{unit} is evaluated as $L_{unit} = 0.010$ pH/μm and $L_{unit} = 0.0099$ pH/μm, respectively. From these L_{unit} values and Eqs. (8) and (9), the depth $h + 2\lambda_L$ is estimated to be 0.34 and 0.33 μm for aL_S and $(1-a)L_S$, respectively. This difference may be due to the distribution of $h + 2\lambda_L$ on the same SQUID, resulting in the weak dependence of $L_S = aL_S + (1-a)L_S$ on l_{JJ} shown in Fig. 4 against Eq. (10). From our experimental results in Fig. 4, the loop inductance of $L_S = 6.2$ pH with the extra inductance $L_{ext} = 0.90$ pH was obtained. Though two of seven test elements lack a part of data, this does not affect these results.

Fig. 5 is the relationship between the fractional parameters a and the length from JJ to GND l_{JJ}. The experimental values were obtained by dividing the fractional inductance aL_S by the loop inductance L_S. Open circles denote the experimental values of a those were obtained in the range from 0.29 to 0.77 as a function of l_{JJ} ranging from 161 to 466 μm. A solid line is designed a-l_{JJ} relation based on Eq. (10), modified by replacement of L_S and l with aL_S and l_{JJ}, respectively, with $L_{unit} = 0.011$ pH/μm and $L_{ext} = 0$ pH. Fig. 5 indicates that the experimental a is in good agreement with designed one within −3/+10%. Eq. (7) indicates that $1-a$ $(= \eta_{DI})$ should be proportional to $1/f_r$ for keeping Δf_r as constant. From our experimental a, one can say that η_{DI} is varied from 0.23 to 0.71 with the deviation from the designed η_{DI} of less than −3/+10%. This is equivalent to the fact that our present design on the direct coupling covers frequency region for readout f_r with the ratio of $0.71/0.23 = 3.1$ that covers typical 4–8 GHz band of cryogenic HEMT amplifiers with the same accuracy as η_{DI}. Moreover, from the

DOI: 10.1587/elex.14.20170271
Received March 21, 2017
Accepted May 2, 2017
Publicized May 22, 2017
Copyedited June 10, 2017

geometry of our present SQUID, this ratio is expected to be increased to $(1-0.04)/(1-0.87) = 7.4$ where the fractional parameter a could be varied in the range from 0.04 to 0.87, that covers completely 4–16 GHz band of recent HEMT amplifiers [16].

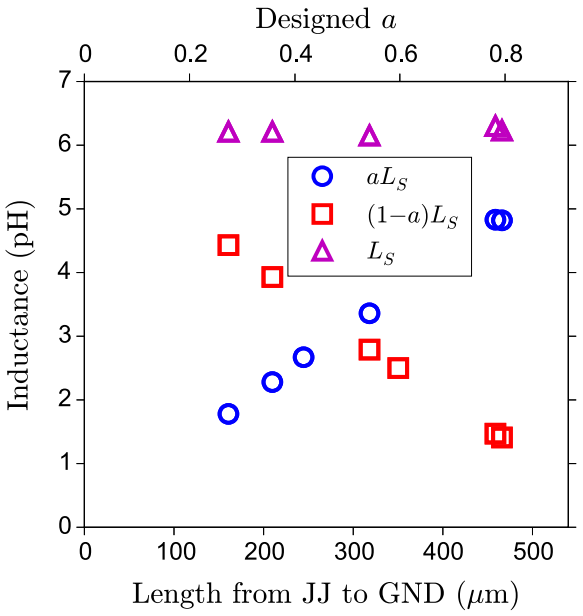

Fig. 4. Experimental SQUID inductance vs. l_{JJ} and designed a. Blue circle, red square and magenta triangle denote aL_S, $(1-a)L_S$ and L_S, respectively.

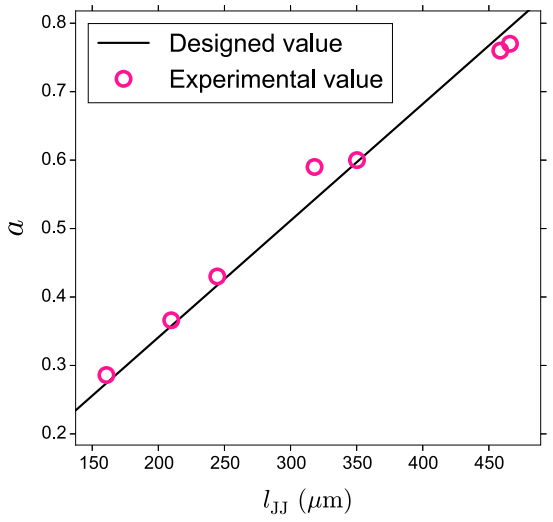

Fig. 5. Experimental (open-circles) and designed (solid line) fractional parameter a vs. l_{JJ}. Due to the experimental setup, two of seven test elements, $l_{JJ} = 245$ and 350 µm, were evaluated only one side of fractional SQUID loop inductance. Therefore, the other sides of those were estimated by assuming that the total SQUID loop inductance is 6.2 pH, which is the average value calculated from the others.

DOI: 10.1587/elex.14.20170271
Received March 21, 2017
Accepted May 2, 2017
Publicized May 22, 2017
Copyedited June 10, 2017

4 Conclusion

In the direct SQUID-resonator coupling, we succeeded in changing the fractional parameters a, keeping the identical structure, shape and dimension of the SQUID for all pixels except only for varying the position of the ground via. We characterized each fractional inductance aL_S and $(1-a)L_S$ as a function of the length from the junction to the ground via, and we experimentally showed that a in the range from 0.29 to 0.77 were in agreement with those of designed within $-3/+10\%$. This covers the frequency band of typical 4–8 GHz cryogenic HEMT amplifiers. Our approach is expected to be valid for more range of a, that confirmation should be a future work.

Acknowledgments

This work was supported by "JSPS KAKENHI Grant Numbers JP15H02251 and 26220703." The microwave SQUID multiplexers were fabricated in the clean room for analog – digital superconductivity (CRAVITY) of National Institute of Advanced Industrial Science and Technology (AIST) in Tsukuba, Japan. We would like to greatly thank Michiyo Isaka for the chip fabrication, and Tomoya Irimatsugawa for the beneficial discussion.

DOI: 10.1587/elex.14.20170271
Received March 21, 2017
Accepted May 2, 2017
Publicized May 22, 2017
Copyedited June 10, 2017